Supplementary Materials: Magnetic Behavior of Carboxylate and β-Diketonate Lanthanide Complexes Containing Stable Organometallic Moieties in the Core-Forming Ligand

Nikolay N. Efimov, Pavel S. Koroteev, Andrey V. Gavrikov, Andrey B. Ilyukhin, Zhanna V. Dobrokhotova and Vladimir M. Novotortsev

Table S1. Crystal data and structure refinement for **3** and **4**.

Identification Code	3	4
Empirical formula	$C_{52}H_{60}Dy_2Fe_4N_2O_{18}S_4$	$C_{95}H_{106}Dy_2Fe_6O_{18}S_4$
Formula weight	1677.66	2324.13
Temperature, K	150(2)	150(2)
Wavelength, Å	0.71073	0.71073
Crystal system	Triclinic	Triclinic
Space group	P-1	P-1
a, Å	10.9663(4)	11.8542(18)
b, Å	12.4258(4)	12.1760(17)
c, Å	13.2417(4)	18.746(3)
α, °	63.6850(10)	75.162(5)
β, °	89.4910(10)	75.706(5)
γ, °	66.1940(10)	61.132(5)
Volume, Å^3	1447.62(8)	2266.1(6)
Z	1	1
D (calc), Mg/m^3	1.924	1.703
μ, mm^{-1}	3.740	2.719
F(000)	830	1172
Crystal size, mm	0.24 × 0.2 × 0.18	0.1 × 0.06 × 0.02
θ range, °	2.043, 31.541	2.272, 27.127
Index ranges	−16 ⩽ h ⩽ 16 −18 ⩽ k ⩽ 18 −19 ⩽ l ⩽ 19	−15 ⩽ h ⩽ 15 −15 ⩽ k ⩽ 15 −23 ⩽ l ⩽ 23
Reflections collected	20907	20655
Independent reflections, Rint	8990, 0.0280	9678, 0.0728
Completeness to θ = 25.242°	99.9%	99.9%
Absorption correction	Semi-empirical from equivalents	Semi-empirical from equivalents
Max,. min. transmission	0.7457, 0.574	0.7455, 0.5554
Refinement method	Full-matrix least-squares on F^2	Full-matrix least-squares on F^2
Data/restraints/parameters	8990/12/386	9678/20/524
Goodness-of-fit	0.965	0.959
*R*1, *wR*2 [*I* > 2sigma(*I*)]	0.0271, 0.0654	0.0565, 0.0878
*R*1, *wR*2 (all data)	0.0336, 0.0689	0.1089, 0.1024
Largest diff. peak and hole, e.Å^{-3}	1.344, −1.241	1.121, −1.203

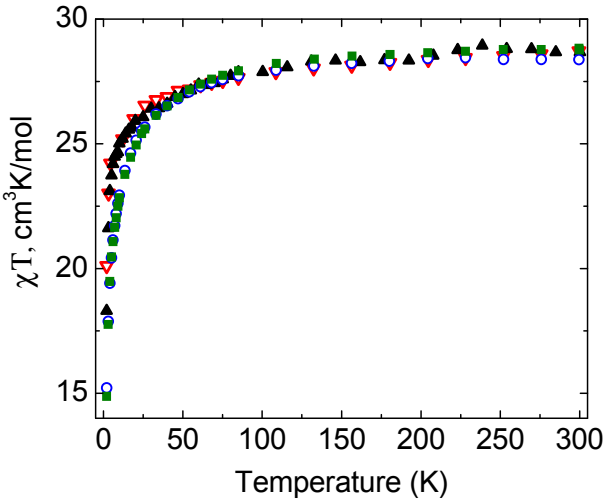

Figure S1. Plots of χT vs. temperature for **1**–**4** (▽—**1** [18], ▲—**2**, o—**3**, ■—**4**). The measurements were carried out in an external magnetic field H = 5000 Oe.

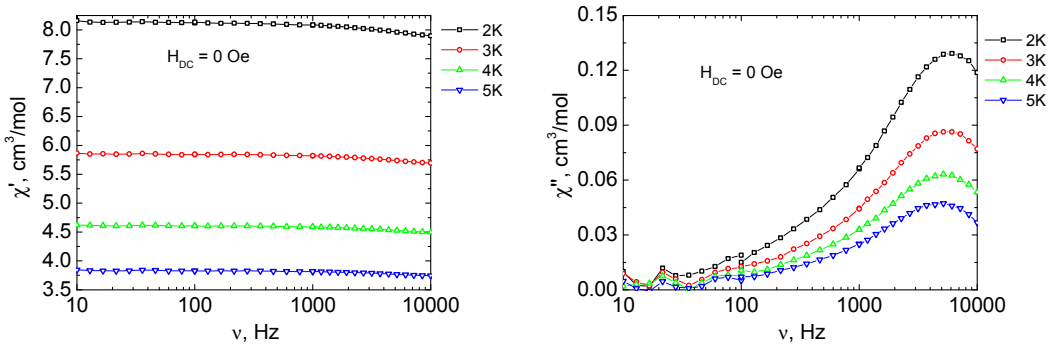

Figure S2. Frequency dependences of in-phase (χ′, **a**) and out-of-phase (χ″, **b**) parts of the ac susceptibility, between 2 and 6 K, for [$Dy_2(O_2CCym)_6(DMSO)_4$] (**1**) in zero dc field (this study). Solid lines are visual guides.

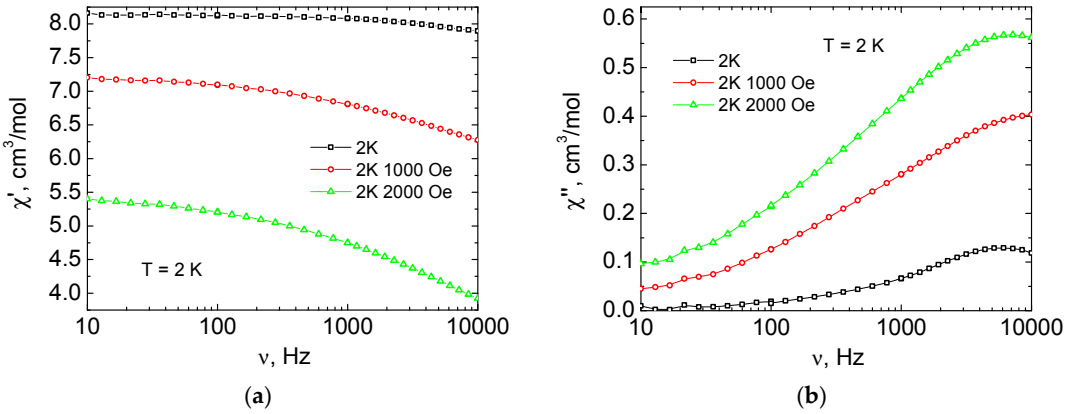

Figure S3. Frequency dependences of in-phase (χ′, **a**) and out-of-phase (χ″, **b**) parts of the ac susceptibility, at 2 K, for [$Dy_2(O_2CCym)_6(DMSO)_4$] (**1**) in zero, 1000 and 2000 Oe dc-field (this study). Solid lines are visual guides.

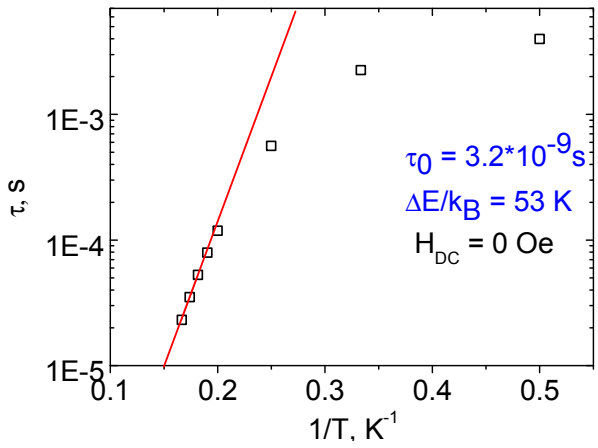

Figure S4. τ vs. T^{-1} plot for $[Dy_2(O_2CCym)_4(NO_3)_2(DMSO)_4]$ (**2**) in zero magnetic field. Solid red line is the best fit to the Arrhenius law ($\tau_0 = 3.2 \cdot 10^{-9}$ s, $\Delta E/k_B = 53$ K) (this study).

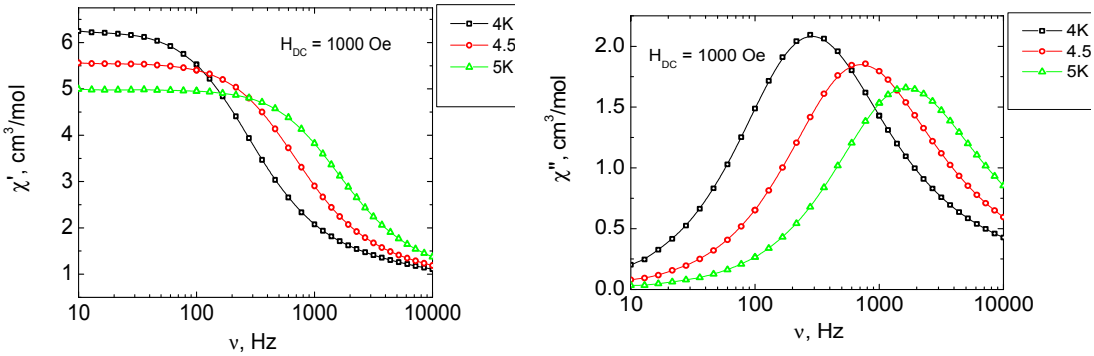

Figure S5. Frequency dependences of in-phase (χ′, **a**) and out-of-phase (χ″, **b**) parts of the ac susceptibility, between 4 and 5 K, for $[Dy_2(O_2CCym)_4(NO_3)_2(DMSO)_4]$ (**2**) in 1000-Oe dc field (this study). Solid lines are visual guides.

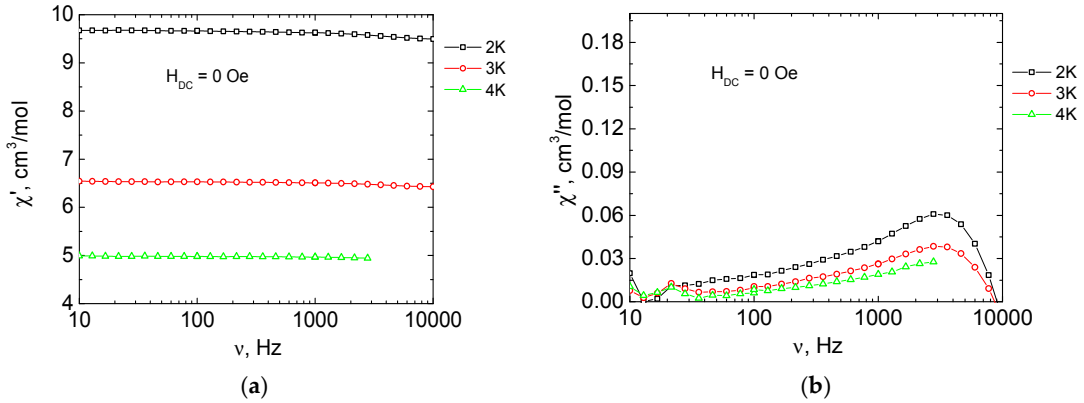

Figure S6. Frequency dependences of in-phase (χ′, **a**) and out-of-phase (χ″, **b**) parts of the ac susceptibility, between 2 and 4 K, for $[Dy_2(O_2CFc)_4(NO_3)_2(DMSO)_4]$ (**3**) in zero dc field (this study). Solid lines are visual guides.

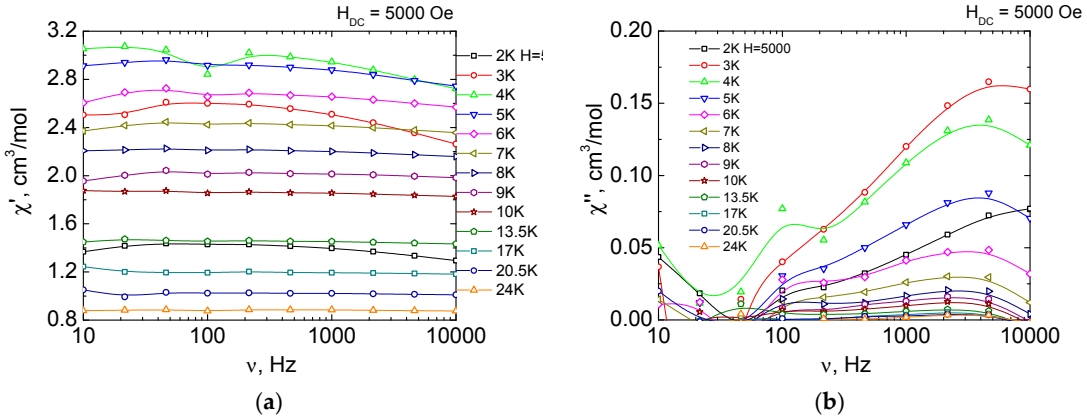

Figure S7. Frequency dependences of in-phase (χ′, **a**) and out-of-phase (χ″, **b**) parts of the ac susceptibility, between 2 and 24 K, for $[Dy_2(O_2CFc)_4(NO_3)_2(DMSO)_4]$ (**3**) in 5000-Oe dc field (this study). Solid lines are visual guides.

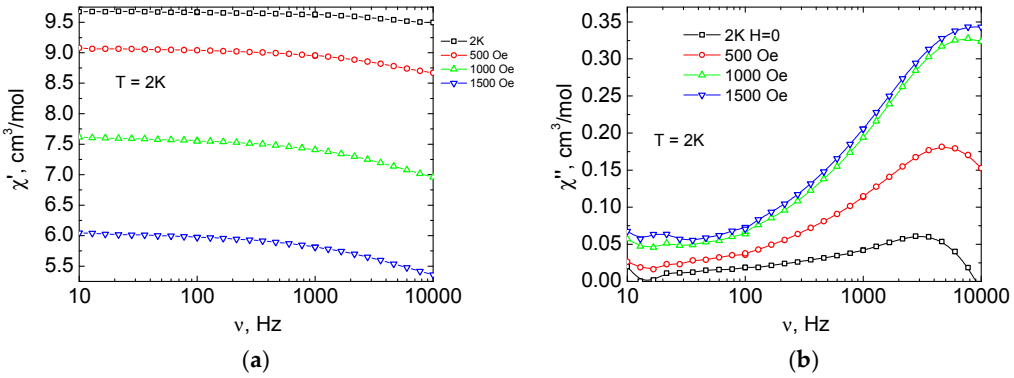

Figure S8. Frequency dependences of in-phase (χ′, **a**) and out-of-phase (χ″, **b**) parts of the ac susceptibility, at 2 K, for $[Dy_2(O_2CFc)_4(NO_3)_2(DMSO)_4]$ (**3**) in zero, 500, 1000 and 1500 Oe dc-field (this study). Solid lines are visual guides.

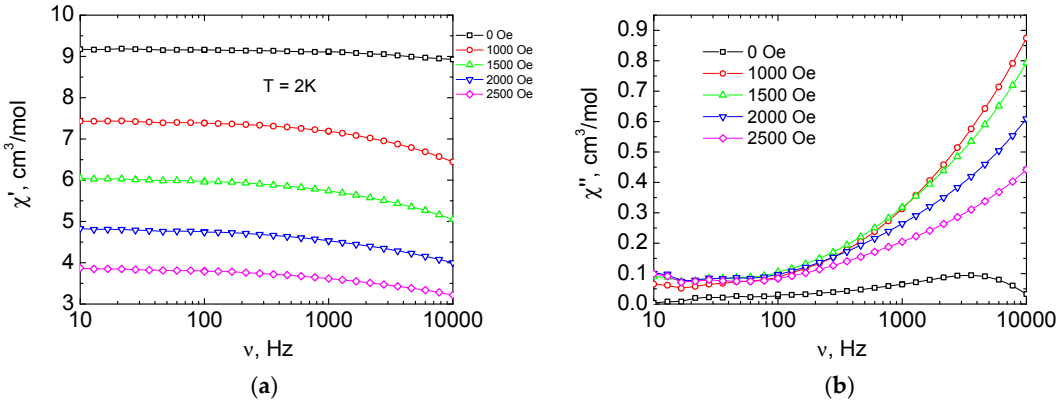

Figure S9. Frequency dependences of in-phase (χ′, **a**) and out-of-phase (χ″, **b**) parts of the ac susceptibility, at 2 K, for $[Dy_2(O_2CFc)_6(DMSO)_2(H_2O)_2]$ (**4**) in zero, 1000, 1500, 2000 and 2500 Oe dc-field (this study). Solid lines are visual guides.

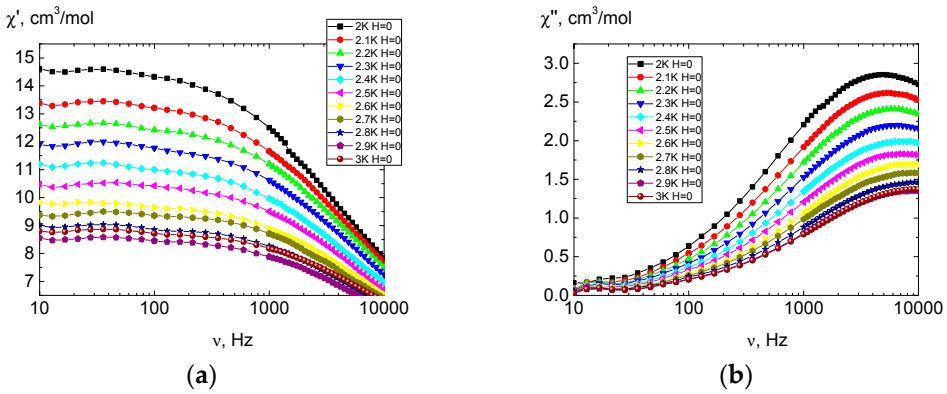

Figure S10. Frequency dependences of in-phase (χ′, **a**) and out-of-phase (χ″, **b**) parts of the ac susceptibility for [Dy(η²-O₂CCym)₂(μ-O₂CCym)₄Dy(H₂O)₄]$_n$ (**5**) (H_{DC} = 0 Oe) [21].

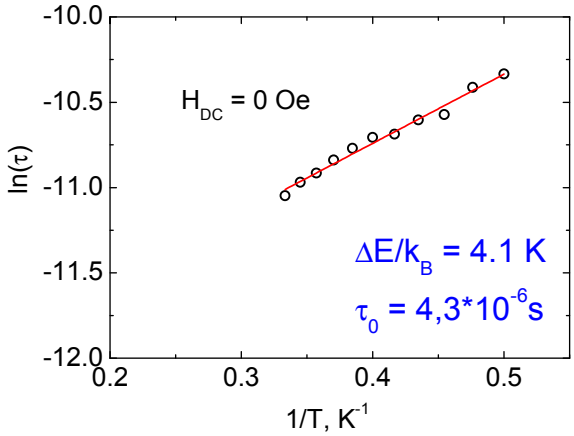

Figure S11. Plot of ln(τ) vs. 1/*T* [Dy(η²-O₂CCym)₂(μ-O₂CCym)₄Dy(H₂O)₄]$_n$ (**5**) obtained from frequency dependences of χ″ in zero magnetic field [21].

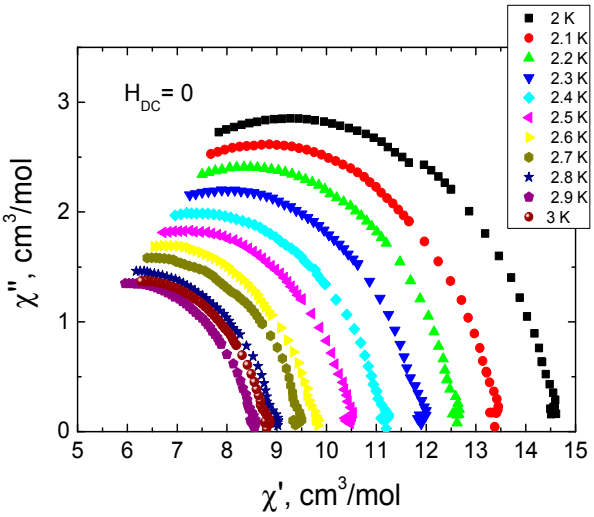

Figure S12. Cole-Cole dependence for [Dy₂(O₂CCym)₆(H₂O)₄]$_n$ (**5**) (H_{DC} = 0 Oe) [21].

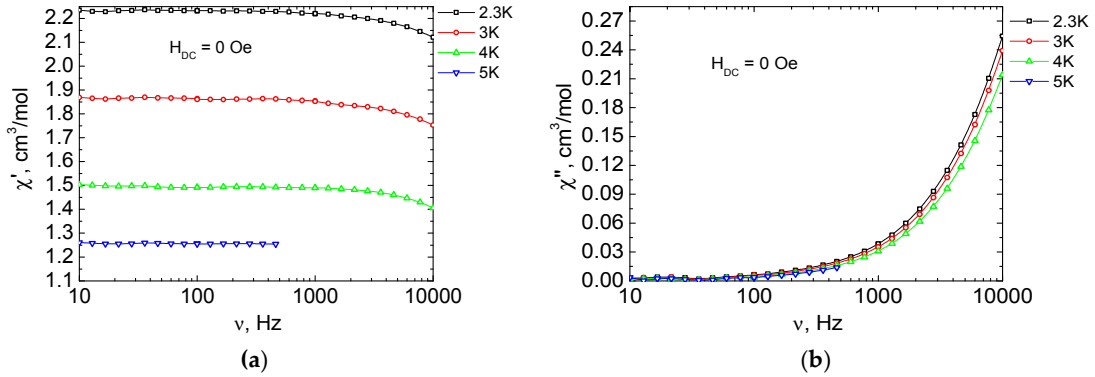

Figure S13. Frequency dependences of the in-phase (**a**) and out-of-phase (**b**) parts of the ac susceptibility of [Dy(CymCO$_2$)(acac)$_2$(H$_2$O)]$_n$ (**6**) (H_{DC} = 0 Oe) (this study).

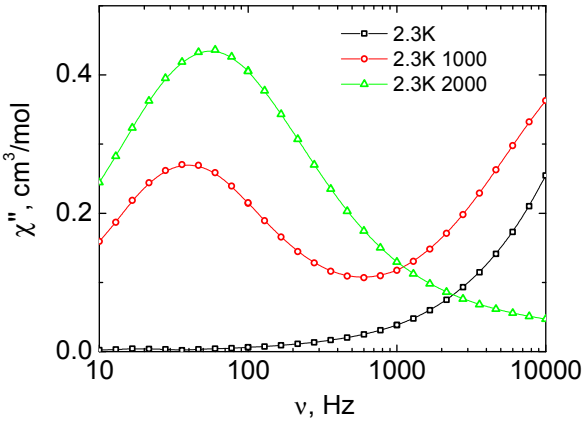

Figure S14. Frequency dependences of out-of-phase (χ″) parts of the ac susceptibility at 2.3 K, for [Dy(CymCO$_2$)(acac)$_2$(H$_2$O)]$_n$ (**6**) in in zero, 1000 and 2000 Oe dc-field. Solid lines are visual guides (this study).

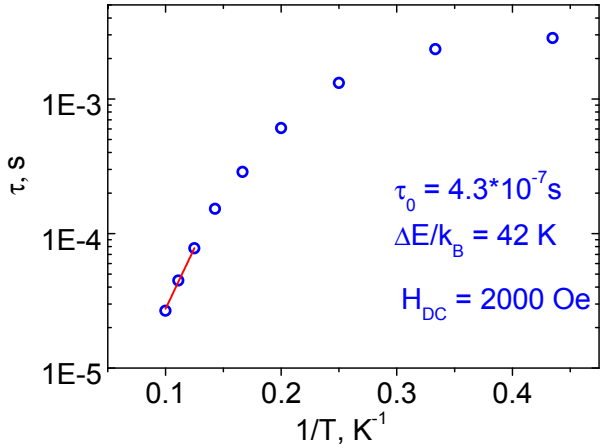

Figure S15. τ vs. T^{-1} plot for [Dy(CymCO$_2$)(acac)$_2$(H$_2$O)]$_n$ (**6**) in 2000 Oe dc-field. Solid red line is the best fit to the Arrhenius law (this study).